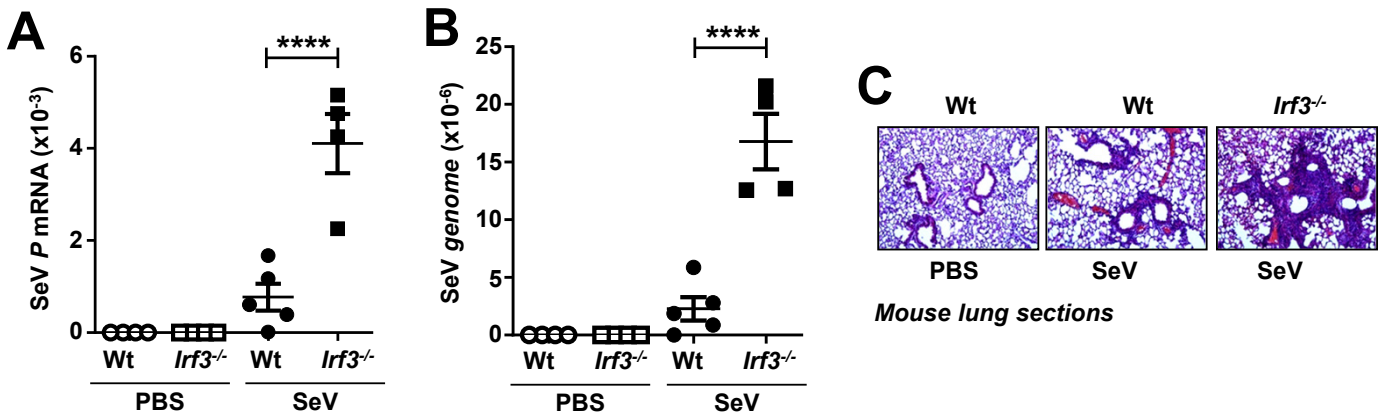

Fig S1. Increased viral replication and inflammatory response in *Irf3*$^{-/-}$ mice in response to SeV infection. (A, B) Wt or *Irf3*$^{-/-}$ mice were PBS-treated or infected with SeV, and the lungs were analyzed for viral RNA levels by qRT-PCR 5 dpi. **(C)** The H&E staining was performed on the lung sections of the PBS-treated and SeV-infected mice 5 dpi. The data represent mean ± SEM, n = 3-5 for each mouse genotype and for each condition, as shown, * represents $p<0.05$.

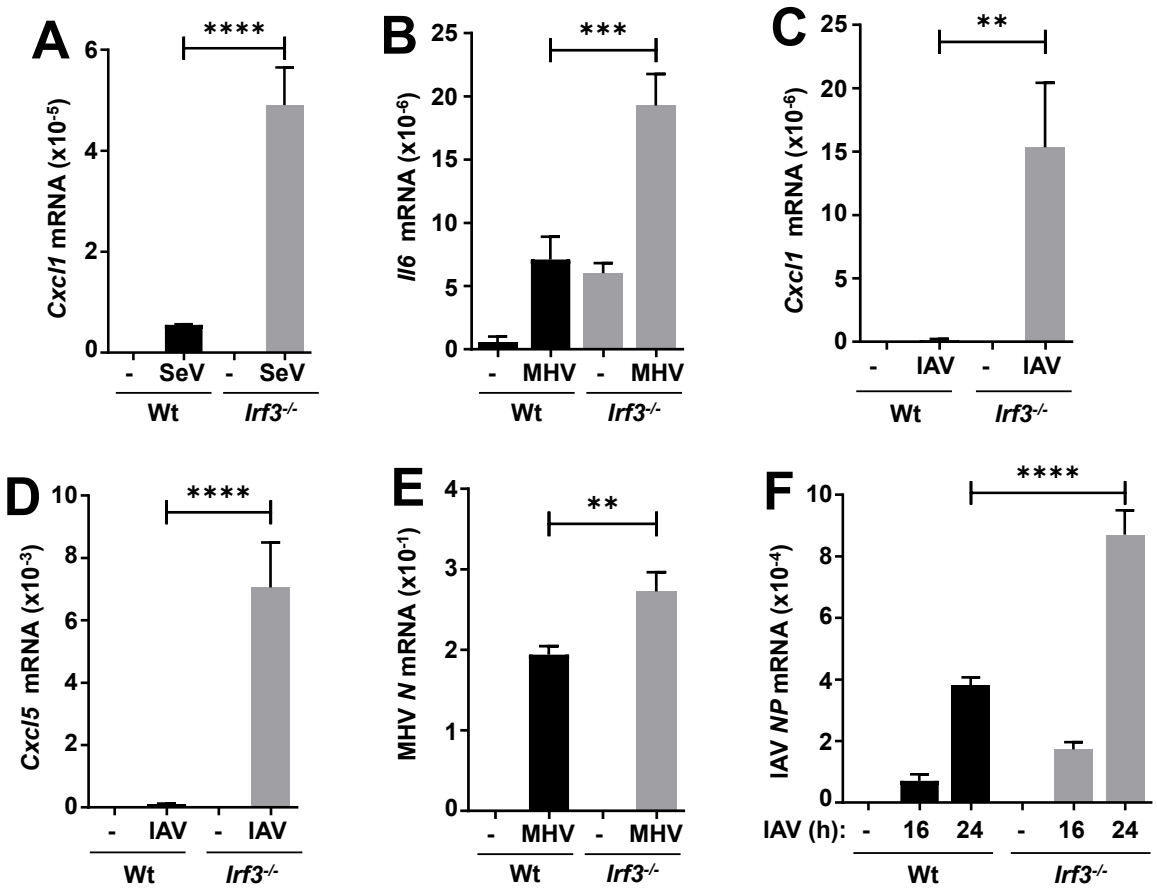

Fig S2. Increased inflammatory gene expression in *Irf3*$^{-/-}$ mouse macrophages upon virus infection. (A-F) Wt or *Irf3*$^{-/-}$ iBMDMs were infected with SeV (A, for 4 hpi), MHV (B, E, 16 h), or IAV (C, D, 16 hpi, F, as indicated), and the mRNAs of various inflammatory target genes (A-D) or viral genes (E, F) were analyzed by qRT-PCR. The results are representative of three experiments; the data represent mean ± SEM, * represents $p<0.05$.

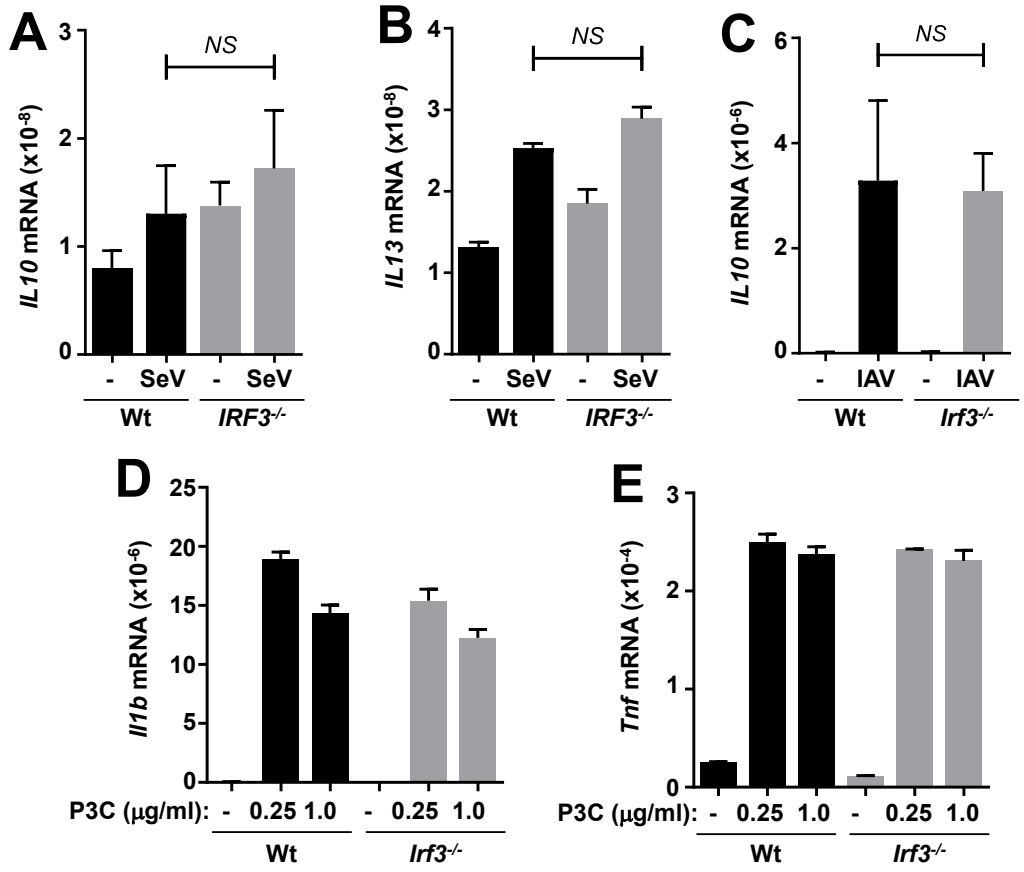

Fig S3. Virus-induced anti-inflammatory genes or TLR2-induced pro-inflammatory genes are not elevated in IRF3-deficient cells. (A, B) Wt and *IRF3*$^{-/-}$ HT1080 cells were infected with SeV (for 4 hpi) and *IL10* and *IL13* mRNA levels was analyzed by qRT-PCR. **(C)** Wt and *Irf3*$^{-/-}$ cells iBMDMs were infected with IAV (for 16 hpi) and the mRNA levels of *Il10* was analyzed by qRT-PCR. **(D, E)** Wt or *Irf3*$^{-/-}$ iBMDMs were treated with TLR2 ligand (Pam3CSK4, P3C) at the indicated doses for 8h, when the *Il1b* and *Tnf* mRNA levels were analyzed by qRT-PCR. The results are representative of three experiments; the data represent mean ± SEM, * represents $p<0.05$.

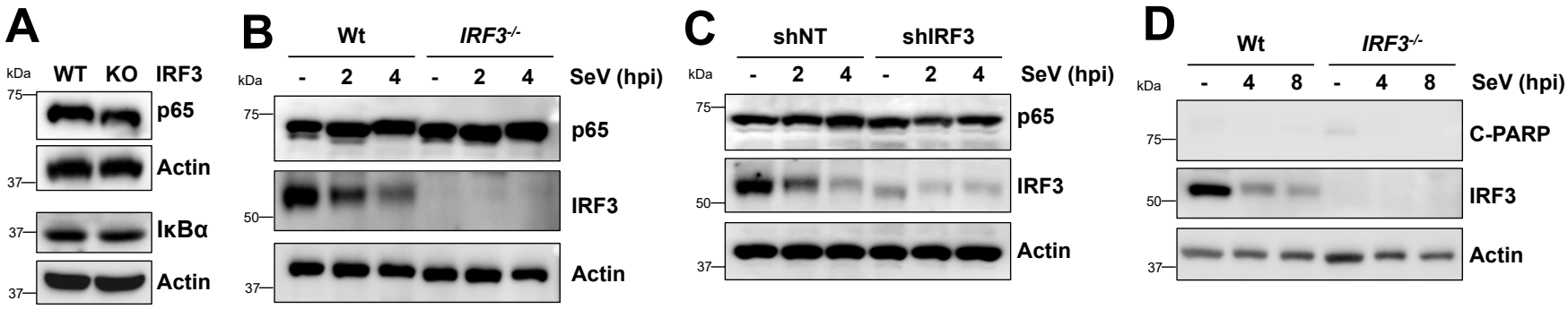

Fig S4. IRF3 deficiency does not cause increased expression of NF-κB-p65 protein expression or apoptotic cell death. (A) Expression of endogenous NF-κB-p65 and IκBα proteins were analyzed in Wt and *IRF3*$^{-/-}$ (KO) HT1080 cells by immunoblot. **(B-D)** Wt, *IRF3*$^{-/-}$ (B, D), or shIRF3 (C) cells were infected with SeV for the indicated time, when the NF-κB-p65 and IRF3 (B, C) or cleaved PARP (C-PARP, D) levels were analyzed by immunoblot. The results are representative of three experiments.

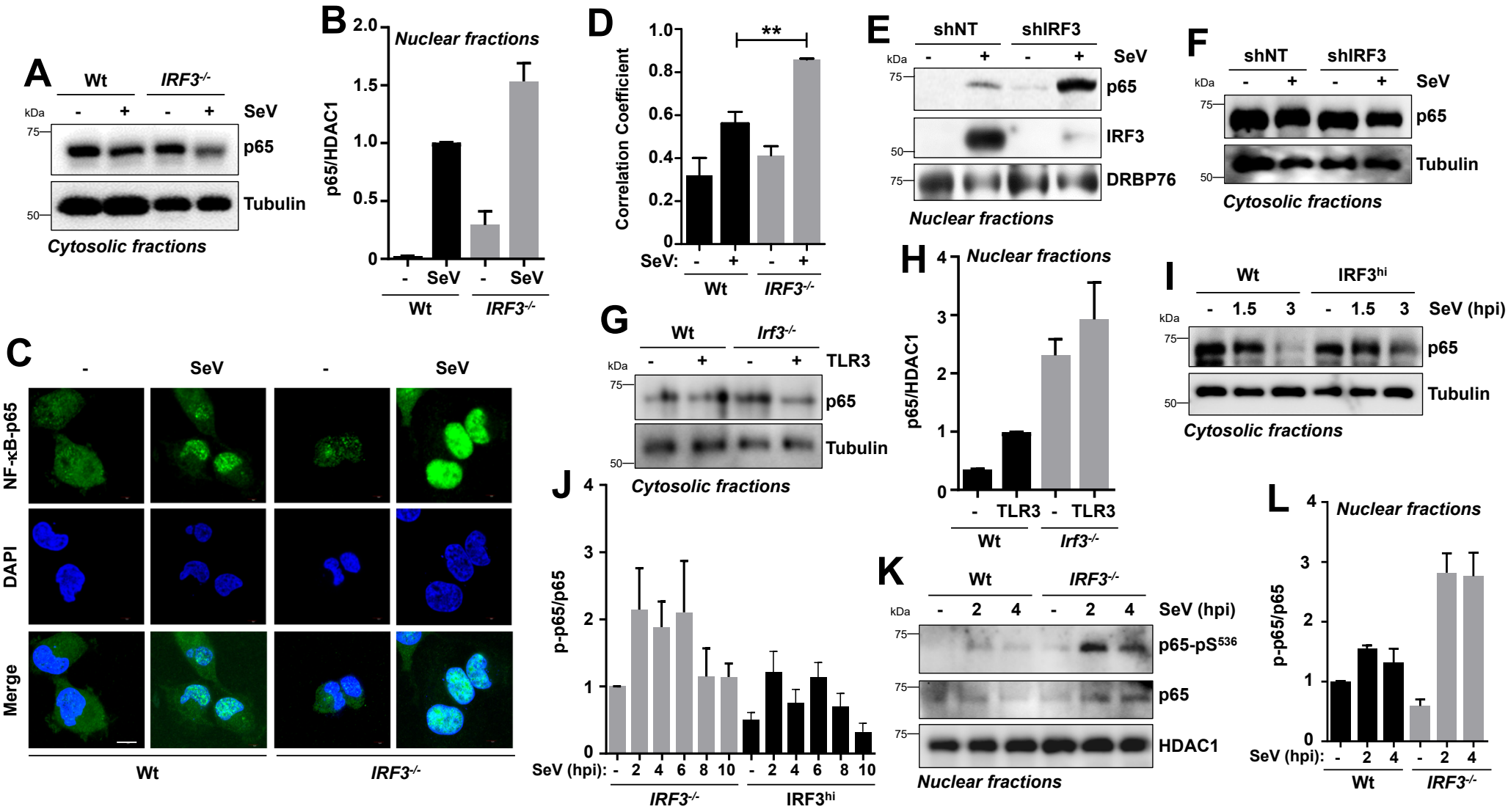

Fig S5. IRF3 deficiency causes increased NF-κB-p65 nuclear translocation. (A) The cytosolic fractions of Wt or *IRF3*$^{-/-}$ HT1080 cells were analyzed for p65 upon SeV infection (for 2h) by immunoblot. **(B)** Densitometric analyses of the nuclear fractions in Fig 5A. **(C, D)** Confocal microscopy of NF-κB-p65 in Wt or *IRF3*$^{-/-}$ HT1080 cells, upon SeV infection 2 hpi (C). The Pearson's correlation coefficient values were calculated from 10-20 cells using three images for each dataset (D). **(E, F)** HT1080 cells, expressing shRNA against IRF3 or a non-targeting (NT) sequence, were infected with SeV for 2h, when the nuclear and cytosolic fractions were analyzed for NF-κB-p65 and IRF3, by immunoblot. **(G)** The cytosolic fractions of Wt or *Irf3*$^{-/-}$ iBMDMs were analyzed for p65 upon polyI:C stimulation (TLR3, for 2h) by immunoblot. **(H)** Densitometric analyses of the nuclear fractions in Fig 5B. **(I)** The cytosolic fractions of Wt or IRF3^{hi} HT1080 cells were analyzed for p65 upon SeV infection (for 2h) by immunoblot. **(J)** Densitometric analyses of the nuclear fractions in Fig 5D. **(K, L)** The nuclear fractions from Wt or *IRF3*$^{-/-}$ HT1080 cells were analyzed for phospho-p65 (on Ser^{536}) upon SeV infection (at the indicated time) by immunoblot and densitometric analyses were performed (L). HDAC1 and DRBP76 are markers of nuclear fractions, tubulin is a marker of cytosolic fractions. The results are representative of three experiments; the data represent mean ± SEM, scale bar is 10 μm, * represents $p<0.05$.

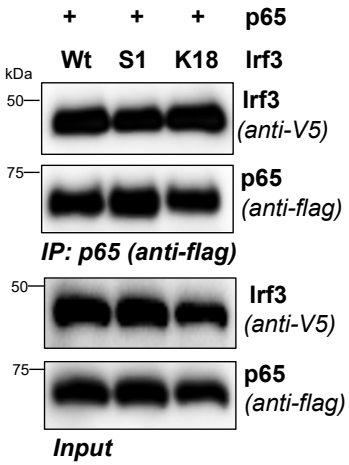

Fig S6. Transcription and RIPA-inactive IRF3 mutants interact with NF-κB-p65. Co-IP analyses of NF-κB-p65 with Wt or mutants of mouse Irf3 in SeV-infected HEK293T cells 2 hpi The results are representative of three experiments.

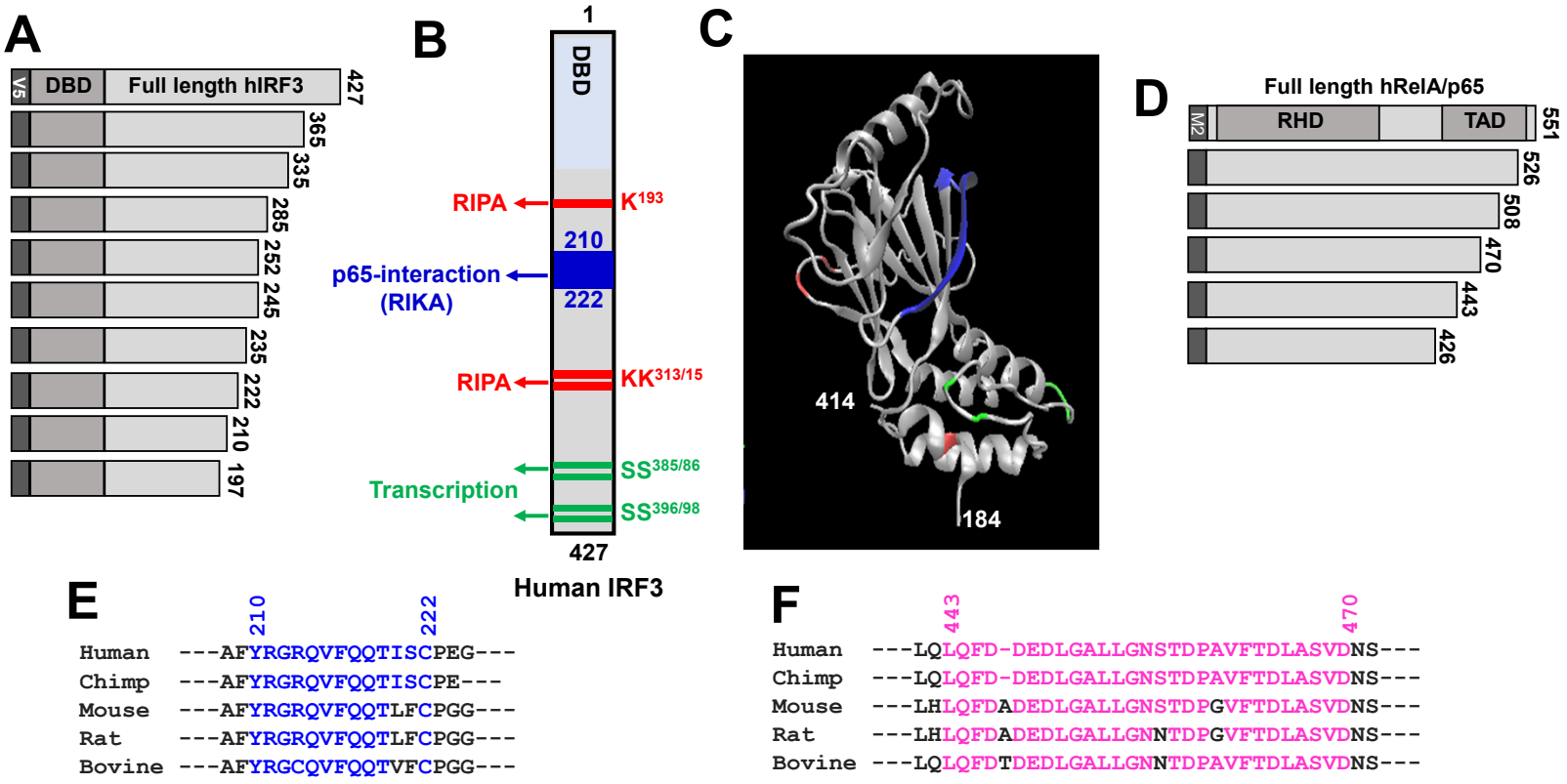

Fig S7. Mapping the interacting domain of IRF3 with NF-κB-p65. (A) Wt (full length) or the C-terminal deletion mutants of V5-IRF3 are shown. **(B, C)** A cartoon showing the critical domains and residues of IRF3 for pathway-specific functions (B), and a 3D-structural model showing the domains and residues involved (using colors as in B) in these functions (C). **(D)** A cartoon showing the Wt (full length) and the deletion mutants of Flag-NF-κB-p65. **(E, F)** The alignment of the interacting domains of IRF3 (E) and NF-κB-p65 (F) across multiple species.

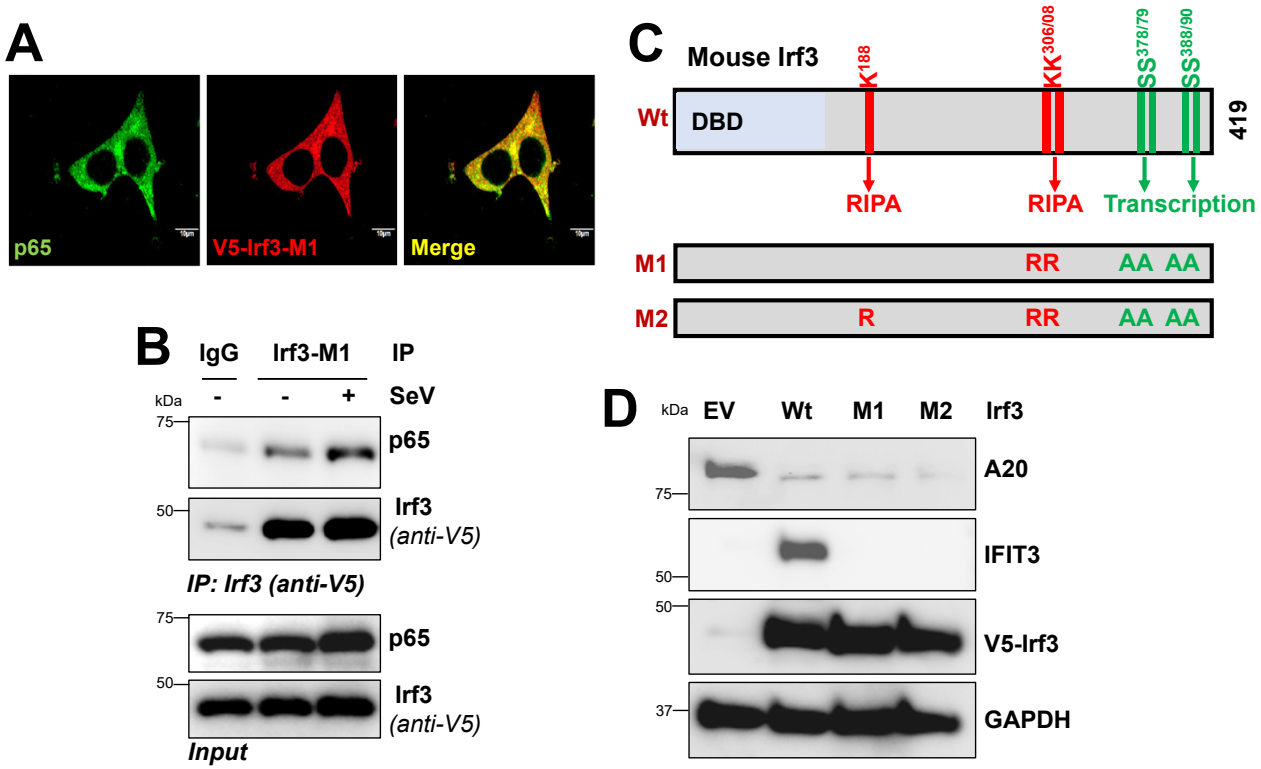

Fig S8. Transcription and RIPA-inactive IRF3 mutants interact with NF-κB-p65 to trigger RIKA. (A) Confocal microscopy of endogenous NF-κB-p65 and V5-Irf3-M1, expressed in *Irf3*$^{-/-}$ iBMDMs, upon SeV infection. **(B)** V5-Irf3-M1-expressing *Irf3*$^{-/-}$ iBMDMs were infected with SeV for 2h and subjected to co-IP analyses for the endogenous NF-κB-p65 and V5-Irf3. **(C)** A cartoon showing mouse Irf3 and its critical residues and domains (DBD, DNA-binding domain) involved in specific functions, and the pathway-specific mutants (Irf3-M1 and Irf3-M2). **(D)** *IRF3*$^{-/-}$ HT1080 cells, ectopically expressing Wt or mutants of Irf3, were analyzed for SeV-induced A20 and IFIT3 expression by immunoblot. EV, empty vector, IgG, mouse-IgG control, scale bar is 10 μm. The results are representative of three experiments.

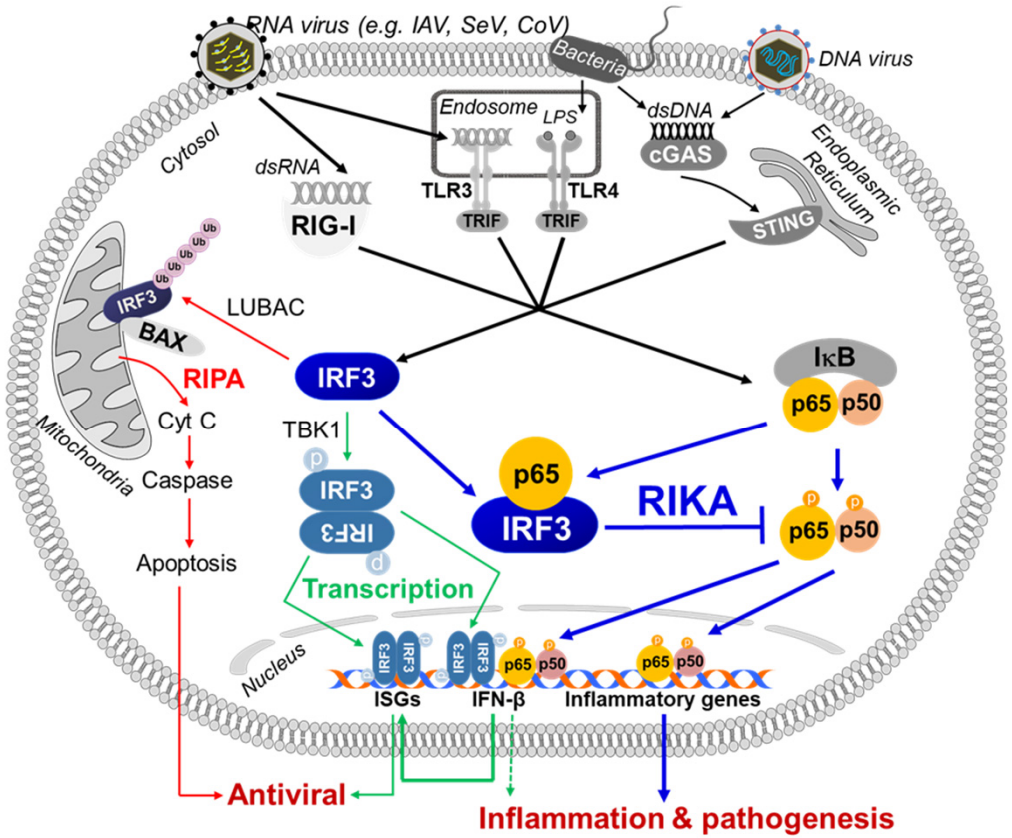

Fig S9. A diagram showing the transcriptional and non-transcriptional activities of IRF3 and their contribution to the optimal IRF3 functions. IRF3 is activated by phosphorylation upon virus infection or non-viral stimulations, e.g., TLR, RLR, STING agonists, and leads to the transcriptional induction of IFNβ and ISGs. In addition, IRF3 can be activated by ubiquitination, leading to the apoptotic pathway (RIPA). We present a new function of IRF3, independent of transcriptional and apoptotic activities, to interact with NF-κB-p65 and suppress the inflammatory gene induction. All functions of IRF3 contribute to the optimal antiviral protection by IRF3.

Table S1: NF-κB-induced genes in shIRF3 (KD) and HT1080 (Wt) (related to Fig 3A)

NF-κB genes	Fold change: sh/Wt
KLK3	196.9929033
IL1A	94.96295172
IL1B	91.4640133
CCL3	87.91478486
SAA2	71.27476863
SERPINA1	45.93270513
BDKRB1	37.96351908
TRAF1	28.24778537
CCL20	26.43912875
SAA1	20.12267502
VCAM1	19.89421722
CSF2	19.25653874
MMP9	19.09260206
TNFAIP2	19.01841279
SERPINA1	14.10842222
HMOX1	13.5813153
SOD2	11.26723576
LTA	9.892589922
CYP7B1	9.76422339
EBI3	9.367252192
WT1	8.076774429
NFKBIE	6.986852872
BCL3	6.728656968
IER3	6.704942085
ADORA2A	6.325605493
TFF3	6.027897897
PRKACA	5.93503615
CYP19A1	4.797237073
CD209	4.726011969
MMP1	4.667810051
CD86	4.144855922
KLF10	3.927415896
IL1RN	3.917471991
SPP1	3.701070682
NFKB2	3.623371378
JUNB	3.602130605
BIRC2	3.585966267
IL8	3.460348937

F8	3.257978518
TNFAIP3	2.894124912
CD44	2.870663071
VEGFC	2.842875892
KLRA1	2.590343509
XDH	2.536365254
EGFR	2.523901768
PTX3	2.49906675
BCL2A1	2.486793963
ST6GAL1	2.388519689
ABCC6	2.37879039
PLK3	2.20888794
GADD45B	2.200838305
CDKN1A	2.194691637
CCND1	2.169038163
CYP27B1	2.165445187
TIFA	2.152993774
ERBB2	2.147598874
PRKCD	2.142779812
RELB	2.107647886
TNF	2.063232069
CD44	2.059770392
GAD1	2.059536049
BCL2L1	2.047113621
F11R	2.037749724
GCLM	2.022333429
ADORA1	2.012507826

Table S2: Fold induction of NF-κB-induced genes

NF-κB genes	Fold induction: sh/Wt
TRAF1	73.19554003
SERPINA1	52.92263536
PRKACA	37.26449849
SAA2	34.21258641
KLK3	33.04454369
SERPINA1	24.27998141
CCL20	18.82830566
IL1B	17.8325929
IL1A	11.26685933
ADORA2A	8.73585222
SOD2	8.520655008
TNFAIP2	8.500042078
F8	7.729624812
IER3	7.002416048
ERBB2	6.750214991
MMP1	6.7126701
KLRA1	6.678493412
LTA	6.023500586
PTX3	5.789770282
CD86	4.846703998
IL1RN	4.798852341
HMOX1	4.625338261
KLF10	4.405793437
BCL3	4.102645875
CD44	3.390627864
CD44	3.390627864
SAA1	3.316628643
TNFAIP3	3.25359055
EBI3	3.236702681
BIRC2	2.93578609
CYP19A1	2.530422275
EGFR	2.368144464
TIFA	2.341340552
MMP9	2.29109528
PLK3	2.066256022
GADD45B	1.994307678
BCL2L1	1.98364452

Table S3: The qRT-PCR primers used in the study

Gene	Primers (Fwd, Rev)
TNFAIP3	CGTCCAGGTTCCAGAACACCATTC, TGCGCTGGCTCGATCTCAGTTG
Tnfaip3	TTTGCTACGACACTCGGAAC, TTCTGAGGATGTTGCTGAGG
IL1a	ACTGCCCAAGATGAAGACCA, CCGTGAGTTTCCCAGAAGAA
Il1a	GTGTTGCTGAAGGAGTTGCCAGAA, TGCACCCGACTTTGTTCTTTGGT
IL1b	AAATACCTGTGGCCTTGGGC, TTTGGGATCTACACTCTCCAGCT
Il1b	ACACATGTTCTCTGGGAAATCGT, AAGTGCATCATCGTTGTTCATACA
IL6	GTAGCCGCCCCACACAGA, CATGTCTCCTTTCTCAGGGCTG
Il6	GACGGCACACCCACCCT, AAACCGTTTTTCCATCTTCTTCTTT
CXCL1	AACCGAAGTCATAGCCACAC, GTTGGATTTGTCACTGTTCAGC
Cxcl1	TGAGCTGCGCTGTCAGTGCCT, AGAAGCCAGCGTTCACCAGA
CXCL5	GAGAGCTGCGTTGCGTTTG, TTTCCTTGTTTCCACCGTCGA
Cxcl5	GCATTTCTGTTGCTGTTCACGCTG, CCTCCTTCTGGTTTTTCAGTTTAGC
SeV P	CAAAAGTGAGGGCGAAGGAGAA, CGCCCAGATCCTGAGATACAGA
SeV genome	ACTGGTCCGGATAAGAAGGC, AGTTCCTGATCAGACCCGTG
MHV N	GCCAAATAATCGCGCTAGAA, CCGAGCTTAGCCAAAACAAG
IAV NP	TGCAAGGTTCAACTCTCCCT, GTTCCGGCTCTCTCTCACTT
TNF	ATGAGCACTGAAAGCATGATCC, GAGGGCTGATTAGAGAGAGGTC
IL10	TCTCCGAGATGCCTTCAGCAGA, TCAGACAAGGCTTGGCAACCCA
IL13	ACGGTCATTGCTCTCACTTGCC, CTGTCAGGTTGATGCTCCATACC
Il10	AAGGCAGTGGAGCAGGTGAA, CCAGCAGACTCAATACACAC
IFIT1	Described before (1)
IFIT3	Described before (1)
IFNB1	Described before (1)
18S	Described before (1)

1. S. Chattopadhyay, T. Kuzmanovic, Y. Zhang, J. L. Wetzel, G. C. Sen, Ubiquitination of the Transcription Factor IRF-3 Activates RIPA, the Apoptotic Pathway that Protects Mice from Viral Pathogenesis. *Immunity* **44**, 1151-1161 (2016).